The Annals of Applied Statistics
2017, Vol. 11, No. 2, 898–918
DOI: 10.1214/17-AOAS1022
© Institute of Mathematical Statistics, 2017

EVALUATION OF THE COOLING TREND IN THE IONOSPHERE USING FUNCTIONAL REGRESSION WITH INCOMPLETE CURVES[1]

BY OLEKSANDR GROMENKO, PIOTR KOKOSZKA AND JAN SOJKA

IBM Research, Colorado State University and Utah State University

We develop a statistical framework to test the hypothesis of the existence of an ionospheric cooling trend related to the global warming hypothesis; both are attributed to the same driver, namely the increased concentration of greenhouse gases. However, the study of a temporal trend in the ionosphere is easier because there are fewer covariates to be taken into account. The hypothesis that a cooling trend in the ionosphere exists has been an important focus of space physics research for over two decades. A central difficulty in reaching broadly agreed—on conclusions has been the absence of data with sufficiently long temporal and sufficiently broad spatial coverage. Complete time series of data that cover several decades exist only in a few separated (industrialized) regions. The space physics community has struggled to combine the information contained in these data, and often contradictory conclusions have been reported based on the analyses relying on one or a few locations. We present a statistical analysis that uses all data, even those with incomplete temporal coverage. It is based on a new functional regression approach that can handle spatially indexed curves whose temporal domain depends on location and may contain gaps. The test statistic combines spatial and temporal dependence in the data and is approximately normally distributed. We conclude that a statistically significant cooling trend exists in the Northern Hemisphere. This confirms the hypothesis put forward in the space physics community over two decades ago.

1. Introduction. This paper is concerned with a long standing problem of space physics research. The increased concentration of greenhouse gases in the upper atmosphere is associated with global warming in the lower troposphere. Roble and Dickinson (1989) suggested that the increasing amounts of these radiatively active gases, mostly CO_2 and CH_4, would lead to a global cooling in the thermosphere. Rishbeth (1990) pointed out that this would result in a thermal contraction of the atmosphere and the global lowering of the ionospheric peak electron density, both in terms of height and absolute value; see Figure 1. The F region peak has been observed for many decades by globally distributed ground–based ionosondes. The ionosonde is a type of radar projecting a spectrum of high-frequencies (HF) vertically into the ionosphere. In principle, these observations

Received March 2014; revised January 2017.

[1]Supported in part by NSF Grant ATM-DMS-0931948.

Key words and phrases. Cooling trend, functional regression, incomplete time series, ionosphere, solar activity, spatial averaging, spatio-temporal modeling.

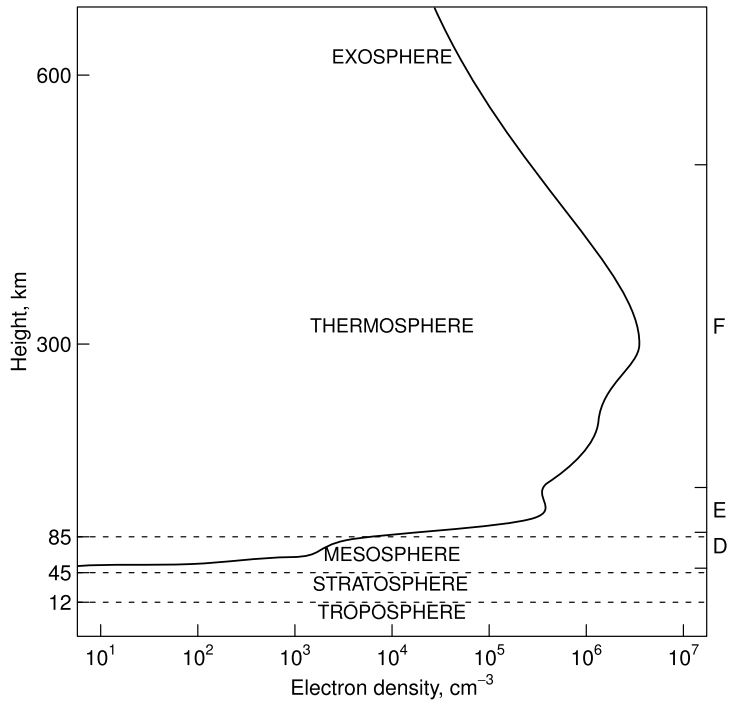

FIG. 1. *Typical profile of the electron density in the day–time ionosphere. The curve shows electron density as a function of height. The right vertical axis indicates the D, E, and F regions of the ionosphere.*

could be used to quantitatively test the hypothesis of Roble and Dickinson (1989). A long term change in the ionosphere can impact space-based navigation (including GPS systems), HF (2-30MHz) radio communication and the operation of low orbit satellites. It is associated with the global warming hypothesis because a physical mechanism for the conjectured cooling trend is also attributable to greenhouse gases.

The ionospheric layer which contains the peak electron density is known as the F2 region (the right-most peak in Figure 1). Ionosonde measurements allow us to compute a critical frequency, denoted foF2. This frequency separates the frequencies returned back to the ionosonde and those that propagate beyond the ionosphere.

There has been extensive space physics research aimed at determining if a decreasing temporal trend in the foF2 frequency indeed exists. Lastovicka et al. (2012) review some of the relevant literature. Long-term changes in the ionosphere are usually described using a linear approximation referred to as the trend. The main problem in its determination is the separation of the solar activity; the solar cycle dominates the shape of the foF2 curves; see Figure 2. A comprehensive overview of statistical methods proposed in the space physics community is given

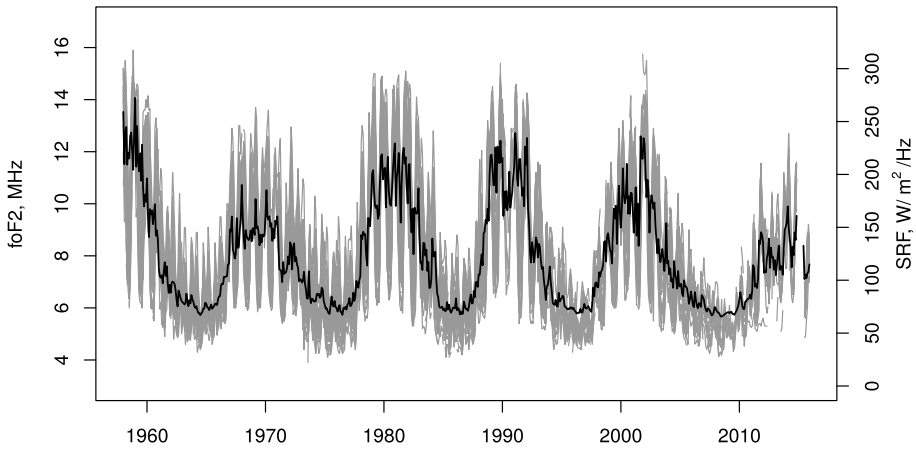

FIG. 2. *Gray lines represent all foF2 records analysed in this paper with the scale on the left-hand side. The black line represents the observed solar radio flux with the scale on the right-hand side.*

in Lastovicka et al. (2006). The main problem from which they suffer is their inability to combine the information from many spatial locations. The usual approach is to calculate trends separately at a number of locations, often using different time periods, and then average these trends to obtain a sense of a global trend; see Bremer et al. (2012) and Bremer and Mielich (2013) for a recent contribution and a discussion of previous work. There has, however, long been a sentiment in the ionospheric physics community, that, in addition to informative exploratory analyses, an inferential statistical framework should be developed to address the question of the existence of long term ionospheric trends; Ulich et al. (2003) stress that to make any trends believable, a suitable statistical modeling, a proper treatment of "errors and uncertainties" is called for.

Our objective is to make a contribution in this direction by developing a statistical inferential framework which allows us to combine incomplete ionosonde records from globally distributed locations and take their spatial dependence into account. The absence of complete records has been a major stumbling block in space physics research to date. Our approach is developed in the framework of functional data analysis: the ionosonde records are viewed as spatially indexed curves which are only partially observed.

There has been an increasing interest in correlated (in particular spatially dependent) functional data. Such data occur in many settings of practical relevance: meteorological and pollution variables at many locations measured over long periods of time, records of brain activity at a number of locations within the brain, economic or health variables indexed by counties, etc. An interested reader is referred to Delicado et al. (2010), Giraldo et al. (2010, 2011, 2012), Nerini et al. (2010), Secchi et al. (2011, 2012), Jiang and Serban (2012), Crainiceanu et al. (2012), Gromenko et al. (2012), Gromenko and Kokoszka (2012, 2013), and Staicu et al.

(2010, 2012). The work of Leibl (2013) is also related as it considers functions whose domain is not fixed. Even though our new functional regression technique has been developed to solve a specific science problem, it is hoped that it will be received with interest as a more broadly applicable tool of functional data analysis.

The data used in this paper are spatio-temporal. There are two natural ways of looking at them: as a collection of time series at fixed locations (the view we take) or as a time series of geostatistical processes; see, for example, Section 6.4 of Cressie and Wikle (2011). The specific approach to be taken depends on the problem at hand. We want to determine if a collection of time series contains a common linear trend, so the first approach is more appropriate. If, for example, the temporal evolution of spatial covariances is of interest, the second approach would be more suitable. The spatio-temporal statistic has been a focus of very intense research over the last two decades, with hundreds of important contributions, in addition of the monograph of Cressie and Wikle (2011), Sherman (2011) and Gelfand et al. (2010) contain very informative chapters with a large number of references.

The remainder of the paper is organized as follows. In Section 2, we introduce the space physics data we work with. Section 3 is devoted to the new statistical methodology we developed to solve the problem outlined above. Some technical aspects of this methodology are explained in the Appendices. In Section 4, we apply these tools to establish, with statistical significance, the existence of a negative foF2 trend in the mid-latitude Northern Hemisphere.

2. The data. To conduct the analysis, we prepare a dataset of foF2 observations. Raw ionosonde data are available at the Space Physics Interactive Data Resource (SPIDR).[2] The resulting dataset represent a collection of time series obtained from different spatial locations. The ionosonde data are very new to the spatio-temporal statistical community, and adequate attention of statisticians may significantly advance the field of space physics. Due to various reasons, the records contain long gaps of missing observations. These gaps often appear at the end or the beginning of the record because some stations started operation a decade or two later than others, and some were shut down. In some cases, a station was shut down and reopened many years later. Shorter periods of missing observations are mostly due to equipment maintenance or replacement. There are also several prepossessed ionosonde datasets freely available online; see, for example, Damboldt and Suessmann (2012).

For the study reported in the paper, we use monthly medians at 12 LT (LT denotes local solar time). At noon, the behavior of the ionosphere is completely dominated by the solar radiation; see Figure 2. At night, the behavior of the ionosphere is complicated, and we postpone the study of the night time data to a more specialized space physics paper. Our statistical study requires the assumption of spatial

[2]http://spidr.ngdc.noaa.gov/spidr/.

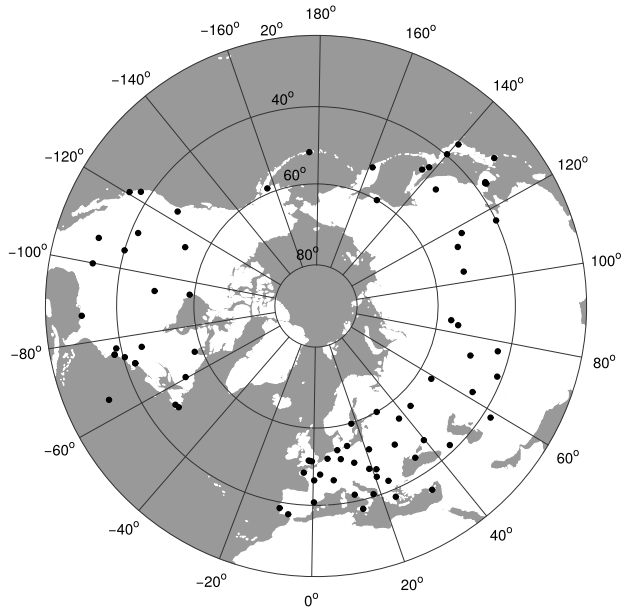

FIG. 3. *Locations of the* 81 *ionosonde stations used in this study, black discs.*

stationarity. To make this assumption reasonable, we focus only on the mid-latitude region located between 30°N and 60°N geographic latitude. The ionosphere can be divided into three regions: equatorial, mid-latitude and polar; see Kelly (2009). It exhibits different electron density profiles in each of these regions, with the profile shown in Figure 1 typical of the mid-latitude region. The reason for choosing the northern hemisphere, rather than the southern hemisphere, is that it contains the longest records with the most extensive spatial coverage. The total number of selected stations is 81; they are shown in Figure 3. The majority of the ionosondes started to operate in 1957, the international geophysical year. We selected the time interval from January 1958 to December 2015, so that the total number of months is 696. While the total number of selected stations is 81, the number of stations available at any specific month never exceeds 50; see Figure 4.

The foF2 curves are used as responses. The main explanatory variable is the observed solar radio flux (SRF), which is a well-established proxy for the solar activity. It is available at SPIDR until the middle of 2012 and at Natural Resources Canada (NRC)[3] October 2004 until present. We combine measurements from the two sources to obtain continuous measurements from January 1958 to December 2015. Other exploratory variables representing different characteristics of the Earth's Magnetic Field (EMF) are obtained using the International Geomagnetic

[3]http://www.nrcan.gc.ca/home

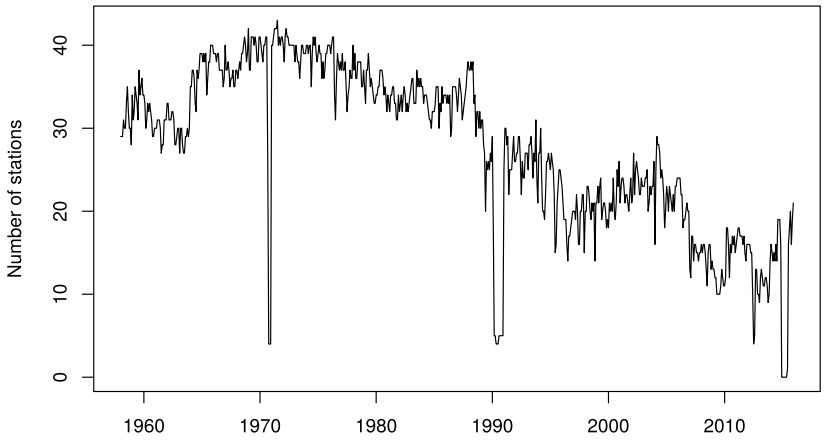

FIG. 4. *Number of available stations in the mid-latitude northern hemisphere.*

Reference Field (IGRF), Thébault et al. (2015). Description of predictors is shown in Table 1 and their summary statistics in Table 2.

3. Statistical model and inference. Let $Y(\mathbf{s}_k; \tau_i)$ be the original record at location $\mathbf{s}_k$, measured from 1958 to 2015, possibly with long gaps. The set of all locations is $\{\mathbf{s}_k, 1 \le k \le K\}$, and the set of time points at which measurements may be available is $\{\tau_i, 1 \le i \le T\}$. In our study, these are months from January 1958 to December 2015. We postulate the following spatio-temporal model:

$$Y(\mathbf{s}_k; \tau) = \mu(\mathbf{s}_k; \tau) + \varepsilon(\mathbf{s}_k; \tau) + \theta(\mathbf{s}_k; \tau), \tag{3.1}$$

where τ is continuous time. The most general form of the mean function μ is specified in Section 3.1. In its simplest form relevant to our space physics problem,

TABLE 1
Predictor definitions

Predictor	**Definition**	**Units of measurement**	**Data source**
SRF	Observed Solar Radio Flux	$W/m^2/Hz$	SPIDR and NRC
D	Declination of the EMF	Deg	IGRF
I	Inclination of the EMF	Deg	IGRF
M	$\sin(I)\cos(I)$	–	IGRF
F	The absolute value of intensity of the EMF	nT	IGRF
F_x	North component of F	nT	IGRF
F_y	East component of F	nT	IGRF
F_z	Down component of F	nT	IGRF
H	Horizontal component of F	nT	IGRF

TABLE 2
Predictor summary statistics in corresponding units

Predictor	Min	25th percentile	Median	75th percentile	Max
SRF	65.60	80.40	110.3	157.00	272.30
D	−32.68	−5.65	0.66	5.80	23.18
I	43.60	59.52	66.22	70.89	83.14
M	0.12	0.31	0.37	0.44	0.50
F	38,022	42,725	45,050	48,095	54,462
F_x	6458	15,497	18,370	21,812	29,252
F_y	−6681	−2222	189	1700	6223
F_z	27,908	37,044	40,602	44,859	54,009
H	6476	15,758	18,610	21,974	29,334

it is

$$\mu(\tau) = \beta_1 + \beta_2\tau + \beta_3 \mathrm{SRF}(\tau), \tag{3.2}$$

where $\mathrm{SRF}(\tau)$ is the solar radio flux; cf. Figure 2. Our interest lies in the estimation of the mean function $\mu(\cdot)$, and testing if it contains a linear trend, that is, testing $H_0 : \beta_2 = 0$. The function $\mu(\cdot)$ is treated as an unknown deterministic functional parameter. The second term, $\varepsilon(\mathbf{s}_k; \tau)$, describes the spatio-temporal variability away from the mean function. Stochastic modeling of this term is needed to develop inferential procedures, and it will be discussed below. The term $\theta(\mathbf{s}_k; \tau)$ represents a random error, which can be associated with measurement error. It exists only at the time of measurement, so using a continuous argument τ is slightly misleading.

3.1. *Modeling the mean function and the spatio-temporal error field.* The mean function is allowed to take the following general form:

$$\mu(\mathbf{s}; \tau) = \sum_{j=1}^{q} \beta_j z_j(\mathbf{s}; \tau). \tag{3.3}$$

The covariates z_j are observed at all time points at which the response curves can be potentially observed (in our application, every month from January 1958 to December 2015). Some covariates, like the SRF, are global, that is, they do not depend on $\mathbf{s}$.

The spatio-temporal field ε is allowed to have a different covariance structure in every year. We split it into annual sections which are denoted by $\varepsilon_n(\mathbf{s}_k; t_i)$: the index $1 \le n \le N$ denotes year, index t_i denotes a month within a year, $\{t_i, 1 \le i \le 12\}$. For a generic location $\mathbf{s}$, we thus have $\varepsilon_n(\mathbf{s}; t_i) = \varepsilon(\mathbf{s}; 12(n-1) + t_i)$. This approach naturally accommodates the annual periodicity of the records. In our implementation, we use the usual calendar years. The covariance surface is then the largest in the middle and tapers off at the edges.

To simplify notation, we assume that the time within a year is rescaled to cover the unit interval [0, 1], so that $t \in [0, 1]$. Each function $\varepsilon_n(\mathbf{s}_k, \cdot)$ is assumed to be a random element of the space $L^2 = L^2([0, 1])$ which satisfies

$$E\|\varepsilon_n(\mathbf{s}_k, \cdot)\|^2 = E\int_0^1 \varepsilon_n^2(\mathbf{s}_k, t)\,dt < \infty. \tag{3.4}$$

We now state assumptions which specify the stochastic structure of the L^2-valued (functional) spatio-temporal field $\{\varepsilon_n(\mathbf{s}_k, \cdot), 1 \le n \le N, 1 \le k \le K\}$. The covariance structure of each field $\varepsilon_n(\cdot; \cdot)$ is restricted by the separability assumption, but is allowed to change with year.

ASSUMPTION 3.1. For each year n, $E\varepsilon_n(\mathbf{s}, t) = 0$ and

$$E\big[\varepsilon_n(\mathbf{s}_k; t_i)\varepsilon_n(\mathbf{s}_\ell; t_j)\big] = \Sigma_n(k, \ell)C_n(t_i, t_j). \tag{3.5}$$

The spatial covariances $\Sigma_n(k, \ell)$ are assumed to depend only on the distance between $\mathbf{s}_k$ and $\mathbf{s}_\ell$.

The spatial and temporal covariance functions in Assumption 3.1 are defined up to multiplicative constants, so we impose the following identifiability condition:

$$\int C_n(t, t)\,dt = \sum_{i=1}^{\infty} \lambda_{ni} = 1, \tag{3.6}$$

where $\lambda_{n1} > \lambda_{n2} > \cdots$ are the eigenvalues of the temporal covariance function C_n.

While separability can be criticized as an excessively strong assumption [see, e.g., Stein (2005)], it is often found acceptable and useful in both theoretical and applied research; see Haas (1995), Genton (2007), Hoff (2011), Paul and Peng (2011), Sun et al. (2012), among many others. In our research, we strived to develop a practically applicable and computationally feasible procedure, admittedly at the cost of some simplifying assumptions. We emphasize that the combined error field $\varepsilon(\cdot, \cdot)$ is not separable. Its covariance structure is determined by our last assumption.

ASSUMPTION 3.2. We assume that the fields $\varepsilon_n(\cdot, \cdot), n \ge 1$ are independent (but not necessarily identically distributed).

It is useful to compare the modeling framework described above with our earlier work presented in Gromenko et al. (2012) and Gromenko and Kokoszka (2013). In those papers, the error field ε was assumed to be a spatially stationary field of functions in $L^2([0, N])$; no splitting into individual years was done. Such an approach leads to the representation:

$$\varepsilon(\mathbf{s}; \tau) = \sum_{j=1}^{\infty} \zeta_j(\mathbf{s})v_j(\tau). \tag{3.7}$$

The new modeling paradigm is dictated by the structure of the data. In Gromenko et al. (2012) and Gromenko and Kokoszka (2013), only slightly over 30 locations and a shorter time period were used because extending the spatial and temporal coverage would include many incomplete records (not just missing values but missing decades). The methodology available at that time did not allow us to deal with such records. For example, integrals of the type $\int Y(\mathbf{s}_\ell;\tau)Y(\mathbf{s}_k;\tau)\,d\tau$ cannot be computed if the records $Y(\mathbf{s}_\ell)$ and $Y(\mathbf{s}_k)$ have practically disjoint supports. The methodology described in the remainder of this section allows us to deal with records containing large gaps by using, in a weighted manner, data at neighboring locations. The methods described in the following sections can be adapted to errors (3.7). The fit of the model curves (3.7) to the observed curves is however poor at some locations over certain time intervals. As a consequence, the estimation of the covariance structure, and so the error variances in the trend test, becomes less precise. In addition to allowing us to deal with large gaps in temporal coverage, the new approach leads to a more precise evaluation of errors because the covariances can change with year, a characteristic we observed in the ionosonde data.

Assumption 3.2 is physically unrealistic because it implies, say, independence of the data in December of year n and January of year $n+1$. It is however computationally convenient. One could consider instead some banded covariance structure with weakly decaying dependence. Such an approach is feasible but computationally more complex, and would not affect the conclusions. The last statement is justified by our numerical experiments in which independence over single years was replaced by independence over periods of two and more years. This impacted the trends and P-values slightly, but not the significance statements.

We conclude this section by formalizing the assumptions on the measurement errors. Analogously to the definition of $\varepsilon_n(\cdot,\cdot)$, we define $\theta_n(\cdot,\cdot)$ to be the field θ restricted to year n.

ASSUMPTION 3.3. For each $n, \mathbf{s}, t$, $\mathrm{Var}[\theta_n(\mathbf{s};t)] < \infty$. The fields $\theta_n(\cdot,\cdot)$ are independent (but not necessarily identically distributed). For each n, the random variables $\theta_n(\mathbf{s},t)$ are independent and identically distributed across $\mathbf{s}$ and t. The field $\theta(\cdot,\cdot)$ is independent of the field $\varepsilon(\cdot,\cdot)$.

3.2. *Estimation in the presence of incomplete records.* The estimation of the components of model (3.1) proceeds through an iterative process described in Algorithm 3.1, which can however be fully understood only after all the steps of the estimation have been explained. The central idea is to pool information from neighboring spatial locations to optimally compensate for the absence of data at certain time intervals at any specific location. In the first step, we completely ignore spatio-temporal dependence and estimate the mean function using ordinary least squares, as explained in Section 3.5. Denoting the resulting estimate by $\hat{\mu}(\mathbf{s}_k,\tau)$, we next compute the residual curves:

$$X(\mathbf{s}_k,\tau) = Y(\mathbf{s}_k,\tau) - \hat{\mu}(\mathbf{s}_k,\tau). \tag{3.8}$$

They will contain gaps. After that, we estimate the spatial and temporal covariances as explained, respectively, in Sections 3.3 and 3.4. Once these estimates have been obtained, we update the estimate of μ, as explained in Section 3.5. The process continues until convergence has been reached. For the estimation of the spatio-temporal covariance, we split $X(\mathbf{s};\tau)$ into annual sub-records, $X_n(\mathbf{s};t)$, where n denotes a year, and t denotes time within a year.

3.3. *Estimation of the spatial covariance.* Following Gromenko et al. (2012), we introduce the *functional variogram*:

$$2\gamma_n(d_{k\ell}) = E\left\{\int \big(X_n(\mathbf{s}_k;t) - X_n(\mathbf{s}_\ell;t)\big)^2\,dt\right\}. \tag{3.9}$$

In this paper, $d_{k\ell}$ is the chordal (Euclidean in R^3) distance between the locations $\mathbf{s}_k$ and $\mathbf{s}_\ell$ on the sphere. A natural estimator of $2\gamma_n(d_{k\ell})$ for *complete records* is

$$2\tilde{\gamma}_n(d_{k\ell}) = \frac{1}{p_{k\ell}} \sum_{P(d_{k\ell})} \frac{1}{L}\sum_{i=1}^{L}\big(X_n(\mathbf{s}_k;t_i) - X_n(\mathbf{s}_\ell;t_i)\big)^2, \tag{3.10}$$

where $P(d_{k\ell})$ is the set of points whose distance to one another is approximately $d_{k\ell}$, and $p_{k\ell}$ is its cardinality. When the records are incomplete, averaging over time can be a source of a severe bias, especially for short records. Thus, preaveraging over time should be avoided. Instead, we perform averaging for *all available squared differences* $(X_n(\mathbf{s}_k;t_i) - X_n(\mathbf{s}_\ell;t_i))^2$, $1 \le i \le L$, for locations which fall into $P(d_{k\ell})$. The resulting estimator is noisy and the corresponding spatial covariance is not necessarily positive definite. We thus fit a valid parametric semivariogram model to the $\tilde{\gamma}_n(d_{k\ell})$, using nonlinear least squares. For the ionosonde data, we found it sufficient to use the Gaussian model

$$\gamma_n(d) = \big(\sigma_n^2 - \sigma_{nv}^2\big)\big(1 - \exp\big(-d^2/\rho_n^2\big)\big) + \sigma_{nv}^2\mathbf{1}_{(0,\infty)}(d), \tag{3.11}$$

and the Exponential model

$$\gamma_n(d) = \big(\sigma_n^2 - \sigma_{nv}^2\big)\big(1 - \exp(-d/\rho_n)\big) + \sigma_{nv}^2\mathbf{1}_{(0,\infty)}(d). \tag{3.12}$$

Several examples of fitted semivariograms for different years are shown in Figure 5. The type of a model is selected based on residual sum of squares (RSS) for each year separately. We also fitted the more complex Matérn model, which has theoretical advantages; see Stein (1999). However, Matérn and the Gaussian models produced practically identical fits in terms of RSS.

Once the parameters σ_n^2, σ_{nv}^2, and ρ_n^2 have been estimated, calculation of the covariance matrix $\mathbf{\Sigma}_n$ is straightforward. It only requires plugging in the distances between locations with *available observations* into the equation for covariance function:

$$\Sigma_n(d) = \sigma_n^2\exp\big(-d^2/\rho_n^2\big) + \sigma_{nv}^2\mathbf{1}_{\{0\}}(d), \tag{3.13}$$

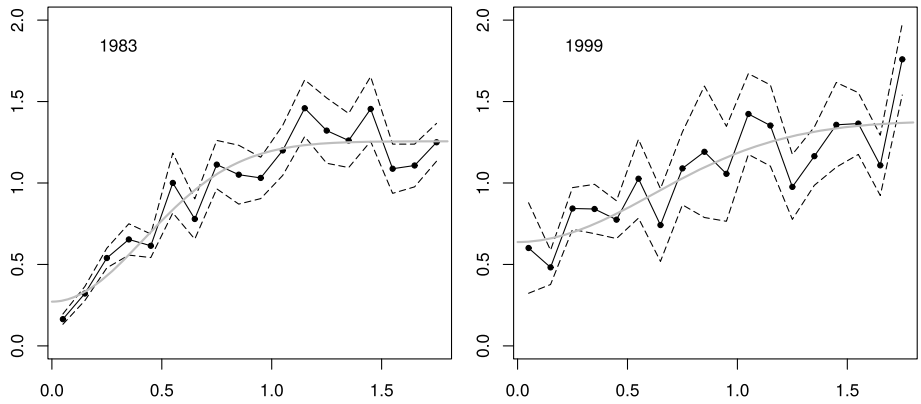

FIG. 5. *Examples of estimated functional semivariograms for several years. Black lines with dots represent estimated semivariograms with* 95% *pointwise confidence intervals, dashed lines. Gray lines represent fits to the selected parametric model, captions at corners indicate the year. Horizontal axes represent distance in radians.*

for the Gaussian model, and

$$\Sigma_n(d) = \sigma_n^2 \exp(-d/\rho_n) + \sigma_{nv}^2 \mathbf{1}_{\{0\}}(d), \tag{3.14}$$

for the Exponential model. It is important to note that full automation of the above procedure is quite difficult, since the "noise" in the data could significantly disturb the estimate of the functional variogram and make the subsequent estimation of the parametric covariance unreliable or impossible at all. One way to stabilize estimation of the functional variogram is to employ robust (highly robust) variogram estimators; see Cressie and Hawkins (1980) and Genton (1998). However, in our case, neither estimator led to a significant improvement. We found that the main source of instabilities are observations that lie far apart. Adjusting the maximal value of the distance $d_{k\ell}$ improves stability of estimation. Such an adjustment affects the estimates only slightly; see Table 4 for details.

We also found that the estimate for the nugget parameter σ_{nv}^2 tends to be smaller than the actual value. Thus, instead of using σ_{nv}^2 from a parametric model we estimate it using residuals directly:

$$\widehat{\sigma}_{nv}^2 = \sum_{k,i} X_n(\mathbf{s}_k, t_i)^2/(P-1) - \widehat{\sigma}_n^2, \tag{3.15}$$

where P is the total number of residuals, and $\widehat{\sigma}_n^2$ is the estimate of sill obtained from a parametric model.

3.4. *Estimation of the temporal covariance.* To determine the statistical significance of the conjectured cooling trend, we need to estimate the temporal covariance surface of the incomplete functional field Y. Due to Assumption 3.2, the

resulting covariance surface is block diagonal: $\mathbf{C} = \operatorname{diag}[\mathbf{C}_1, \ldots, \mathbf{C}_N]$. Before describing our method, we comment on the existing covariance surface estimation procedures. When records are independent and fully observed, the covariance surface is estimated using the sample covariance function; see, for example, Chapter 2 of Horváth and Kokoszka (2012). When records are correlated and complete, one can use one of the estimators proposed in Gromenko et al. (2012), which use projections onto some orthonormal basis. When curves are independent and sparsely observed, the covariance surface may be estimated in a two-step procedure proposed in Yao et al. (2005). The case of independent and identically distributed functions observed with gaps was addressed by Kraus (2015) None of the above methods is applicable to our problem which involves incomplete and correlated curves. However, the methods of Yao et al. (2005) and Kraus (2015) can be extended to take into account spatial dependence, as we now explain.

For fixed i and j, define the scalar field:

$$\psi_n(\mathbf{s}) = \psi_n(\mathbf{s}; t_i, t_j) = X_n(\mathbf{s}; t_i) X_n(\mathbf{s}; t_j). \tag{3.16}$$

By Assumption 3.1, the expectation of $\psi_n(\mathbf{s}_k)$ is approximately equal to $\Sigma_n(k,k)$ $C_n(t_i, t_j)$. The preliminary temporal covariance surface can be estimated up to a constant [cf. (3.6)], as a weighted average:

$$\widetilde{C}_n(t_i, t_j) = \sum_{k=1}^{K} \nu_n(k) \psi_n(\mathbf{s}_k; t_i, t_j), \qquad \sum_{k=1}^{K} \nu_n(k) = 1. \tag{3.17}$$

The weights can be selected to minimize the variance of the estimator, which leads to the following solution:

$$\boldsymbol{\nu}_n = \boldsymbol{\Sigma}_{n\psi}^{-1} \mathbf{1} / (\mathbf{1}^T \boldsymbol{\Sigma}_{n\psi}^{-1} \mathbf{1}), \tag{3.18}$$

where $\boldsymbol{\Sigma}_{n\psi}$ is the covariance matrix with elements $\Sigma_{n\psi}(k,\ell) = \operatorname{Cov}(\psi_n(\mathbf{s}_k), \psi_n(\mathbf{s}_\ell))$. The matrix $\boldsymbol{\Sigma}_{n\psi}$ is difficult estimate due to noisy behavior of the spatial field $\psi_n(\mathbf{s})$. We therefore use the approximation:

$$\operatorname{Cov}\big(\psi_n(\mathbf{s}_k), \psi_n(\mathbf{s}_\ell)\big) \approx \Sigma_n^2(k,\ell) g_n(t_i, t_j). \tag{3.19}$$

This approximation immediately follows from Isserlis' theorem. Indeed,

$$\operatorname{Cov}\big(\psi(\mathbf{s}_k), \psi(\mathbf{s}_\ell)\big) = E\big(\psi(\mathbf{s}_k)\psi(\mathbf{s}_\ell)\big) - E\big(\psi(\mathbf{s}_k)\big) E\big(\psi(\mathbf{s}_\ell)\big). \tag{3.20}$$

The second term on the RHS is

$$E\big(\psi(\mathbf{s}_k)\big) E\big(\psi(\mathbf{s}_\ell)\big) = \Sigma(k,k)\Sigma(\ell,\ell) C^2(t_i, t_j), \tag{3.21}$$

and the first term can be calculated using Isserlis' theorem:

$$\begin{aligned} E\big(\psi(\mathbf{s}_k)\psi(\mathbf{s}_\ell)\big) &= \Sigma(k,k)\Sigma(\ell,\ell) C^2(t_i, t_j) \\ &\quad + \Sigma^2(k,\ell) C(t_i, t_i) C(t_j, t_j) \\ &\quad + \Sigma^2(k,\ell) C^2(t_i, t_j). \end{aligned} \tag{3.22}$$

This leads to

$$\operatorname{Cov}\big(\psi(\mathbf{s}_k), \psi(\mathbf{s}_\ell)\big) = \Sigma^2(k,\ell) g(t_i, t_j) \tag{3.23}$$

with $g(t_i, t_j) = C(t_i, t_i)C(t_j, t_j) - C^2(t_i, t_j)$.

In (3.18), the matrix $\mathbf{\Sigma}_{n\psi}$ can be replaced by the matrix $\mathbf{\Sigma}_n^\star$ with entries $\Sigma_n^2(k,\ell)$. Notice that the multiplication by $g_n(t_i, t_j)$ in (3.19) plays no role due to the cancelation in (3.18). The entries $\Sigma_n(k,\ell)$ of the matrix $\mathbf{\Sigma}_n$ are estimated separately for each year using the method explained above.

3.5. *Regression*. We introduce vector notation. Let $\mathbf{Y}$ be the column vector comprised of $Y(\mathbf{s}_k; \tau_i)$, $\mathbf{z}_j$ the column vector of exploratory variable with index j, $\mathbf{Z} = [\mathbf{z}_1, \mathbf{z}_2, \ldots, \mathbf{z}_q]$, and $\boldsymbol{\beta} = [\beta_1, \beta_2, \ldots, \beta_q]^T$ be the vector of fixed unknown coefficients. The generalized Least Squares (GLS) estimator of $\boldsymbol{\beta}$ is

$$\hat{\boldsymbol{\beta}} = \big(\mathbf{Z}^T \mathbf{\Sigma}^{-1} \mathbf{Z}\big)^{-1} \mathbf{Z}^T \mathbf{\Sigma}^{-1} \mathbf{Y} \tag{3.24}$$

with

$$\operatorname{Var}[\hat{\boldsymbol{\beta}}] = \big(\mathbf{Z}^T \mathbf{\Sigma}^{-1} \mathbf{Z}\big)^{-1}. \tag{3.25}$$

If the errors are uncorrelated, $\mathbf{\Sigma} = \sigma^2 \mathbf{I}$, $\hat{\boldsymbol{\beta}}$ reduces to the OLS:

$$\hat{\boldsymbol{\beta}}_{\text{ols}} = \big(\mathbf{Z}^T \mathbf{Z}\big)^{-1} \mathbf{Z}^T \mathbf{Y}, \tag{3.26}$$

$$\operatorname{Var}[\hat{\boldsymbol{\beta}}_{\text{ols}}] = \big(\mathbf{Z}^T \mathbf{Z}\big)^{-1} \sigma^2. \tag{3.27}$$

The responses $Y(\mathbf{s}_k, \tau_i)$ could, in the absence of any gaps, be available as $81 \times 58 \times 12 = 56{,}376$ data points. Thus, the covariance matrix has a very high dimension: $56{,}376 \times 56{,}376$. Inverting such a large matrix in general is infeasible. However, the *block-diagonal* structure of the covariance matrix allows efficient inversion. Indeed, if $\mathbf{\Sigma} = [\mathbf{\Sigma}_1, \mathbf{\Sigma}_2, \ldots, \mathbf{\Sigma}_N]$, then $\mathbf{\Sigma}^{-1} = [\mathbf{\Sigma}_1^{-1}, \mathbf{\Sigma}_2^{-1}, \ldots, \mathbf{\Sigma}_N^{-1}]$. Now, the elements in (3.24) and (3.25) can be calculated. Let $\mathbf{Z}_n$ and $\mathbf{Y}_n$ be the covariates and ionosonde frequencies for year n, respectively, then

$$\hat{\boldsymbol{\beta}} = \left(\sum_{n=1}^{N} \mathbf{Z}_n^T \mathbf{\Sigma}_n^{-1} \mathbf{Z}_n\right)^{-1} \left(\sum_{n=1}^{N} \mathbf{Z}_n^T \mathbf{\Sigma}_n^{-1} \mathbf{Y}_n\right) \tag{3.28}$$

and

$$\operatorname{Var}[\hat{\boldsymbol{\beta}}] = \left(\sum_{n=1}^{N} \mathbf{Z}_n^T \mathbf{\Sigma}_n^{-1} \mathbf{Z}_n\right)^{-1}. \tag{3.29}$$

Formula (3.29) underestimates the true variability of the estimator because we use an estimated $\mathbf{\Sigma}$. Since we use more than 30 years of data, this effect is small.

Using numerical simulations, we found that the estimator $\hat{\boldsymbol{\beta}}$ is approximately normal even if the functions $Y_n(\mathbf{s}_k)$ are not normally distributed. A heuristic justification of its normality is that it is a weighed sum of a large number of $Y(\mathbf{s}_k, \tau_i)$.

(In the absence of dependence, the weights would be all equal, and the normality of $\hat{\boldsymbol{\beta}}$ would be a consequence of the central limit theorem.) Thus to test $\beta_i = 0$, for a fixed i, we thus assume that the statistic $\hat{\beta}_i / \sqrt{\mathrm{Var}[\hat{\beta}_i]}$ has the standard normal distribution. When we incorporate spatio-temporal dependence, we use (3.28) and (3.29), when spatio-temporal dependence is neglected we use the OLS estimates, (3.26) and (3.27). In either case, the P-value is calculated as

$$P\text{-value} = 2\{1 - \Phi(|\hat{\beta}_i / \sqrt{\mathrm{Var}[\hat{\beta}_i]}|)\}, \tag{3.30}$$

where $\Phi(\cdot)$ is the standard normal distribution function. Due to the underestimation of the variability of $\hat{\beta}$, the actual P-values could be smaller than those implied by formula (3.30). Since the P-values we computed are small and imply the existence of a trend, the actual evidence for its existence may be actually stronger.

Observe that $\hat{\boldsymbol{\beta}}$ could, in principle, be replicated. Such replications would need to reflect not only the distributional variability but also variability due to the spatial and temporal gaps in the data. The latter variability appears difficult to simulate, but might be feasible. An investigation in this direction might lead to bootstrap based inference.

Algorithm 3.1 summarizes the estimation and testing which takes spatio-temporal dependence into account.

ALGORITHM 3.1.

1. Estimate the model coefficient $\hat{\boldsymbol{\beta}}$ without taking into account spatio-temporal dependence using equation (3.26).
2. Produce the residual curves $X(\mathbf{s}; \tau)$ by centering the original records $X(\mathbf{s}; \tau) = Y(\mathbf{s}; \tau) - \hat{\mu}(\mathbf{s}; \tau)$.
3. Estimate spatial covariance as described in Section 3.1 and temporal covariance as described in Section 3.4.
4. Calculate bloc-diagonal spatio-temporal covariance.
5. Estimate the model coefficients $\hat{\boldsymbol{\beta}}$ taking into account spatio-temporal dependence using equation (3.28).
6. Repeat steps 2–5, until convergence is reached.
7. Calculate the statistical significance using (3.30) [and (3.28), (3.29)].

4. Application to the ionosonde data. Before presenting and discussing our results, we note that regression analysis has been extensively used in ionospheric research. In early work, a trend estimate would be obtained at a fixed location with a relatively complete record extending over several decades. Its significance would be tested using the usual t-test. The measurements obtained by the Juliusruh (northeastern Germany) ionosonde which started operation in 1961 have been particularly and extensively studied. It was however soon observed that the sign and/or significance of the trend coefficient would depend on the location and the

TABLE 3

Results of applying different models to ionosonde data without incorporating spatio-temporal dependence. *"Trend" is the estimate of the coefficient of* $z(\tau) = \tau$. *The P-values indicate statistical significance*

Model ID	**Model**	**Trend, 10^{-3} MHz/Year**	**Standard error, 10^{-3} MHz/Year**	***P*-value**
1	SRF	−2.24	0.68	0.001
2	SRF, F	−3.82	0.67	$<10^{-4}$
3	SRF, F_x, F_y, F_z	−3.61	0.61	$<10^{-4}$
4	SRF, H	−4.01	0.62	$<10^{-4}$
5	SRF, F, H	−3.48	0.62	$<10^{-4}$
6	SRF, M	−4.77	0.63	$<10^{-4}$
7	SRF, M, F	−4.09	0.62	$<10^{-4}$
8	SRF, M, F_x, F_y, F_z	−3.41	0.62	$<10^{-4}$
9	SRF, M, H	−3.36	0.62	$<10^{-4}$
10	SRF, M, F, H	−3.50	0.62	$<10^{-4}$

time period. In a recent, most comprehensive up-to-date study, Bremer et al. (2012) estimated trend coefficients at practically all available locations and time periods. Their global analysis uses simple averages of trend estimates available over changing time periods. This leads to a useful global picture based on an exploratory analysis, but the significance of such averaged trends is difficult to assess in the absence of a statistical model.

We now present the results of the application of our spatio-temporal model and testing procedure. The results of analysis in which we neglect spatio-temporal correlation are summarized in Table 3. The mean function specification (3.3) includes various predictors representing solar activity and different parameters of the Earth Magnetic Field (EMF); cf. Table 1. It is difficult to say based on physics which EMF parameters are most relevant, so we used all possible combinations. The resulting estimated trends range from $(-4.77 \text{ to } -2.238) \cdot 10^{-3}$ MHz/Year, and are all statistically significant.

We now turn to testing under our model which includes spatial correlation, that is, we use Algorithm 3.1. The results are shown in Table 4. The maximum lag for variogram estimation affects the results, but the essential conclusion that the trend in ionosonde data is negative and statistically significant remains the same. Compared to the trends in Table 3, the trend values computed using the full Algorithm 3.1 are typically over twice as large (in absolute value). As we will see below, for different time periods, the more precise inference based on the full spatio-temporal model may affect the significance of the trend, and even reverse in sign. An example of the estimated trend superimposed on partial residuals is shown in Figure 6.

TABLE 4

Results of applying different models to ionosonde data with incorporating spatio-temporal dependence. *"Trend" is the estimate of the coefficient of* $z(\tau) = \tau$. *The P-values indicate statistical significance. The three panes show the results for three different values of the maximum distance for functional variogram estimation. The dashes indicate cases in which numerical optimization failed*

Model ID	**Model**	**Trend, 10^{-3} MHz/Year**	**Standard error, 10^{-3} MHz/Year**	***P*-value**
	Maximum distance for functional variogram estimation: 1.4 rad			
1	SRF	−5.10	0.60	$<10^{-4}$
2	SRF, F	–	–	–
3	SRF, F_x, F_y, F_z	−10.48	0.46	$<10^{-4}$
4	SRF, H	−8.58	0.50	$<10^{-4}$
5	SRF, F, H	−8.21	0.47	$<10^{-4}$
6	SRF, M	−8.64	0.58	$<10^{-4}$
7	SRF, M, F	−8.70	0.49	$<10^{-4}$
8	SRF, M, F_x, F_y, F_z	−8.54	0.46	$<10^{-4}$
9	SRF, M, H	−6.72	0.48	$<10^{-4}$
10	SRF, M, F, H	−8.05	0.47	$<10^{-4}$
	Maximum distance for functional variogram estimation: 1.6 rad			
1	SRF	−5.85	0.60	$<10^{-4}$
2	SRF, F	−9.60	0.71	$<10^{-4}$
3	SRF, F_x, F_y, F_z	−11.52	0.46	$<10^{-4}$
4	SRF, H	−8.75	0.48	$<10^{-4}$
5	SRF, F, H	−8.19	0.46	$<10^{-4}$
6	SRF, M	−10.08	0.55	$<10^{-4}$
7	SRF, M, F	−11.94	0.48	$<10^{-4}$
8	SRF, M, F_x, F_y, F_z	−8.44	0.47	$<10^{-4}$
9	SRF, M, H	−8.82	0.46	$<10^{-4}$
	Maximum distance for functional variogram estimation: 1.8 rad			
1	SRF	−4.74	0.65	$<10^{-4}$
2	SRF, F	−9.82	0.70	$<10^{-4}$
3	SRF, F_x, F_y, F_z	−10.36	0.48	$<10^{-4}$
4	SRF, H	−9.26	0.48	$<10^{-4}$
5	SRF, F, H	−10.41	0.47	$<10^{-4}$
6	SRF, M	−10.37	0.55	$<10^{-4}$
7	SRF, M, F	−12.31	0.49	$<10^{-4}$
8	SRF, M, F_x, F_y, F_z	−11.22	0.48	$<10^{-4}$
9	SRF, M, H	−11.83	0.47	$<10^{-4}$
10	SRF, M, F, H	–	–	–

Our conclusion (significant negative trend) agrees with the hypothesis of Roble, Dickinson and Rishbeth discussed in Section 1. While a negative trend in the foF2 frequency in the mid-latitude northern hemisphere cannot be quantitatively con-

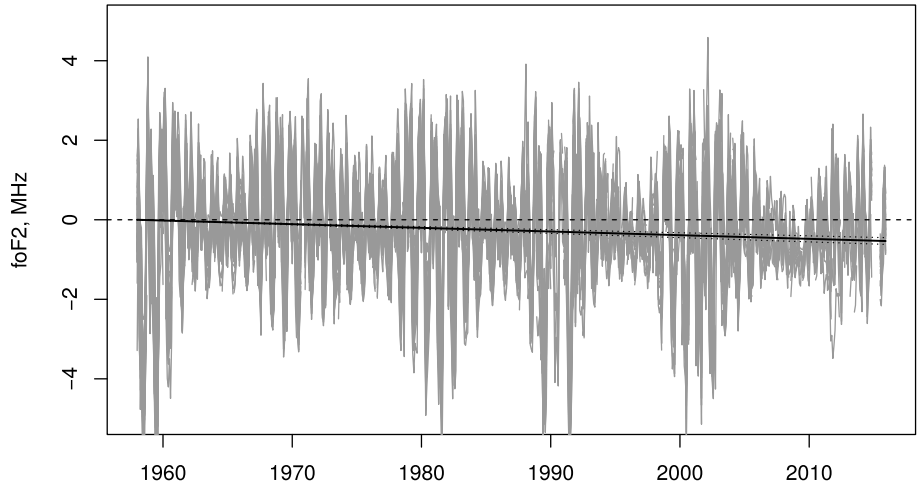

FIG. 6. *Gray lines represent all foF*2 *partial residuals for model with ID* 4 *in Table* 4, $Y(\mathbf{s};\tau) - \beta_1 - \beta_3 SRF(\tau) - \beta_4 H$. *The black line represents the estimated trend together with* 95% *confidence intervals* (*dotted lines*). *The dashed horizontal line is added for visual convenience.*

nected with the magnitude of the hypothesized/observed global warming in the near surface troposphere, there might be some association due to a common driver: the increased concentration of greenhouse gases. The study of a temporal trend in the ionosphere is easier because there are fewer covariates to be taken into account: the important ones are the solar activity, geomagnetic activity, and regional decadal changes in the direction and strength of the internal magnetic field. Terrestrial surface temperature measured at specific locations over a hundred years is impacted by the solar activity but also by many more factors, for example, by urbanization and deforestation, which may produce spurious trends, if not accounted for.

As Bremer et al. (2012), we now show how the conclusion depends on the total length of the time interval used in the estimation and testing. To do this, we fix the interval length, L, and determine the trend for all possible intervals of length L. Figure 7 shows signs of estimated trends as well as their statistical significance for model with ID 4 in Tables 3 and 4. Both models, without and with spatio-temporal correlation, lead to the same conclusion when L is sufficiently large. When the interval length, L, is less then 30 years, depending on the position one may obtain positive and negative trends. However, when the interval is more than 30 years, the estimated trend is consistently negative (except a few points located at the edge). A similar observation was made by Bremer et al. (2012) using exploratory analysis. A key difference between the two approaches is that when using the more recent data, the spatio-temporal modeling approach tends to indicate negative trend more consistently than the approach which ignores spatial dependence. This lends further support to the possibility of anthropogenic origin of the trend. Another useful insight obtained from Figure 7 is that even if the trend is estimated using

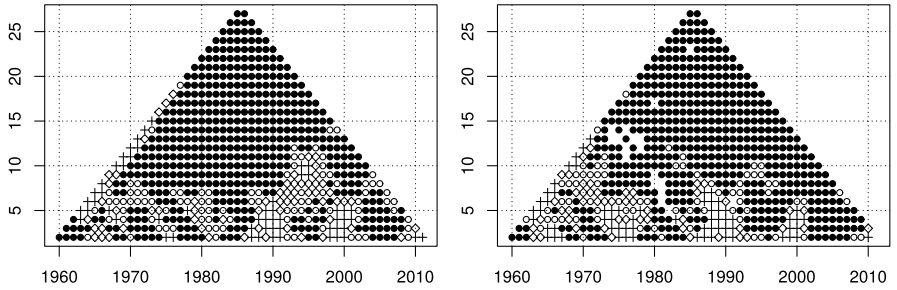

FIG. 7. *Vertical axes represent the half length* $(L/2)$ *of a time interval for trend determination in years, horizontal axes represent the position of the center of a time interval in years. Discs represent negative statistically significant trends, circles represent negative insignificant trends, crosses represent positive statistically significant trends, and empty diamonds represent positive statistically insignificant trends. Left panel: spatio-temporal correlation is neglected. Right panel: spatio-temporal correlation is included. Empty areas represents regions where model has failed to converge.*

a statistical model (rather than by simple averaging of trends), one still obtains a mixture of positive and negative trends, depending on the time interval used to assess it. This explains the apparently contradictory findings reported in space physics literature. Our statistical analysis suggests that the findings of positive, negative, or no trend based on different spatial regions and time intervals may, at least to some extent, reflect the sampling variability of the data.

A contribution of this paper is the development of a statistical framework in which the spatial dependence of ionosonde records and their temporal structure, whose most pronounced feature is long gaps, are taken into account. Within the statistical model we formulated, it is possible to test the significance of a global cooling trend in the ionosphere. In broadest terms, the novelty of our approach consists in applying a statistical test to the whole data set, rather than separately to each segment, and then combining the results in some way, approaches which prevail in related space physics research. This paper contributes to a very large body of space physics research by assessing the cooling hypothesis within this framework. Our conclusions broadly validate those arrived at by many space physics researchers and support the existence of such a trend. However, this view is not universally shared, and a longer period of observation may modify this conclusion. Our estimation and testing methodology is relevant in this context. Many ionosonde observatories have been closed, so gaps in future records may even increase. Our methodology is clearly not the last word in this field, and it is hoped that the present paper will draw interest from the statistics community to this problem. For example, Bayesian approaches might provide different tools, and it would be interesting to see what conclusions they would lead to. While not directly relevant to the space physics problem we have studied, some related recent contributions are Luttinen and Ilin (2009, 2012), Bakar and Sahu (2015) and Yang et al. (2016).

SUPPLEMENTARY MATERIAL

Supplementary material: Evaluation of the cooling trend in the ionosphere using functional regression with incomplete curves (DOI: 10.1214/17-AOAS1022SUPP; .zip). The Supplementary Material contains the code and data used in this paper.

REFERENCES

BAKAR, K. and SAHU, S. (2015). spTimer: Spatio-temporal Bayesian modeling using R. *J. Stat. Softw.* **63** 1–32.

BREMER, J., DAMBOLDT, T., MIELICH, J. and SUESSMANN, P. (2012). Comparing long-term trends in the ionospheric F2—Region with two different methods. *Journal of Atmospheric and Solar-Terrestrial Physics* **77** 174–185.

CRAINICEANU, C. M., STAICU, A.-M., RAY, S. and PUNJABI, N. (2012). Bootstrap-based inference on the difference in the means of two correlated functional processes. *Stat. Med.* **31** 3223–3240. MR2993623

CRESSIE, N. and HAWKINS, D. M. (1980). Robust estimation of the variogram. I. *J. Int. Assoc. Math. Geol.* **12** 115–125. MR0595404

CRESSIE, N. and WIKLE, C. K. (2011). *Statistics for Spatio-Temporal Data*. Wiley, Hoboken, NJ. MR2848400

DAMBOLDT, T. and SUESSMANN, P. (2012). Consolidated Database of worldwide measured monthly medians of ionospheric characteristics foF2 and M(3000)F2. INAG Bulletin on the Web, INAG-73. Available at www.ips.gov.au/IPSHosted/INAG/web-73/index.html.

DELICADO, P., GIRALDO, R., COMAS, C. and MATEU, J. (2010). Statistics for spatial functional data: Some recent contributions. *Environmetrics* **21** 224–239. MR2842240

GELFAND, A. E., DIGGLE, P., GUTTORP, P. and FUENTES, M., eds. (2010). *Handbook of Spatial Statistics*. Chapman & Hall/CRC, Boca Raton, FL.

GENTON, M. G. (1998). Highly robust variogram estimation. *Math. Geol.* **30** 213–221. MR1610687

GENTON, M. G. (2007). Separable approximations of space–time covariance matrices. *Environmetrics* **18** 681–695. MR2408938

GIRALDO, R., DELICADO, P. and MATEU, J. (2010). Continuous time-varying kriging for spatial prediction of functional data: An environmental application. *J. Agric. Biol. Environ. Stat.* **15** 66–82. MR2755385

GIRALDO, R., DELICADO, P. and MATEU, J. (2011). Ordinary kriging for function-valued spatial data. *Environ. Ecol. Stat.* **18** 411–426. MR2832903

GIRALDO, R., DELICADO, P. and MATEU, J. (2012). Hierarchical clustering of spatially correlated functional data. *Stat. Neerl.* **66** 403–421. MR2983302

GROMENKO, O. and KOKOSZKA, P. (2012). Testing the equality of mean functions of ionospheric critical frequency curves. *J. R. Stat. Soc. Ser. C. Appl. Stat.* **61** 715–731. MR2993506

GROMENKO, O. and KOKOSZKA, P. (2013). Nonparametric inference in small data sets of spatially indexed curves with application to ionospheric trend determination. *Comput. Statist. Data Anal.* **59** 82–94. MR3000043

GROMENKO, O., KOKOSZKA, P., ZHU, L. and SOJKA, J. (2012). Estimation and testing for spatially indexed curves with application to ionospheric and magnetic field trends. *Ann. Appl. Stat.* **6** 669–696. MR2976487

HAAS, T. C. (1995). Local prediction of a spatio-temporal process with an application to wet sulfate deposition. *J. Amer. Statist. Assoc.* **90** 1189–1199.

HOFF, P. D. (2011). Separable covariance arrays via the Tucker product, with applications to multivariate relational data. *Bayesian Anal.* **6** 179–196. MR2806238

HORVÁTH, L. and KOKOSZKA, P. (2012). *Inference for Functional Data with Applications*. Springer, New York. MR2920735

JIANG, H. and SERBAN, N. (2012). Clustering random curves under spatial interdependence with application to service accessibility. *Technometrics* **54** 108–119. MR2929427

KELLY, M. C. (2009). *The Earth's Ionosphere*, 2nd ed. Academic Press, San Diego, CA.

KRAUS, D. (2015). Components and completion of partially observed functional data. *J. R. Stat. Soc. Ser. B. Stat. Methodol.* **77** 777–801. MR3382597

LASTOVICKA, J., SOLOMON, S. C. and QIAN, L. (2012). Trends in the neutral and ionized atmosphere. *Reviews of Space Physics* **168** 113–145.

LASTOVICKA, J., MIKHAILOV, A. V., ULICH, T., BREMER, J., ELIAS, A., ORTIZ DE ADLER, N., JARA, V., ABBARCA DEL RIO, R., FOPPIANO, A., OVALLE, E. and DANILOV, A. (2006). Long term trends in foF2: A comparison of various methods. *Journal of Atmospheric and Solar-Terrestrial Physics* **68** 1854–1870.

LIEBL, D. (2013). Modeling and forecasting electricity spot prices: A functional data perspective. *Ann. Appl. Stat.* **7** 1562–1592. MR3127959

LUTTINEN, J. and ILIN, A. (2009). Variational Gaussian-process factor analysis for modeling spatio-temporal data. In *Advances in Neural Information Processing Systems* 22 (Y. Bengio, D. Schuurmans, J. D. Lafferty, C. K. I. Williams and A. Culotta, eds.) 1177–1185. Curran Associates, Red Hook, NY.

LUTTINEN, J. and ILIN, A. (2012). Efficient Gaussian process inference for short-scale spatio–temporal modeling. In *Proceedings of the International Conference on Artificial Intelligence and Statistics* **22**. JMLR W&CP.

MIELICH, J. and BREMER, J. (2013). Long-term trends in the ionospheric F2 region with different solar activity indices. *Annals of Geophysics* **31** 291–303.

NERINI, D., MONESTIEZ, P. and MANTÉ, C. (2010). Cokriging for spatial functional data. *J. Multivariate Anal.* **101** 409–418. MR2564350

PAUL, D. and PENG, J. (2011). Principal components analysis for sparsely observed correlated functional data using a kernel smoothing approach. *Electron. J. Stat.* **5** 1960–2003. MR2870154

RISHBETH, H. (1990). A greenhouse effect in the ionosphere? *Planetary and Space Science* **38** 945–948.

ROBLE, R. G. and DICKINSON, R. E. (1989). How will changes in carbon dioxide and methane modify the mean structure of the mesosphere and thermosphere? *Geophysical Research Letters* **16** 1441–1444.

SECCHI, P., VANTINI, S. and VITELLI, V. (2011). A clustering algorithm for spatially dependent functional data. *Procedia Environmental Sciences* **7** 176–181.

SECCHI, P., VANTINI, S. and VITELLI, V. (2012). Bagging Voronoi classifiers for clustering spatial functional data. *International Journal of Applied Earth Observation and Geoinformation* **22** 53–64.

SHERMAN, M. (2011). *Spatial Statistics and Spatio-Temporal Data*: *Covariance Functions and Directional Properties*. Wiley, Chichester. MR2815783

STAICU, A.-M., CRAINICEANU, C. and CARROLL, R. J. (2010). Fast methods for spatially correlated multilevel functional data. *Biostatistics* **11** 177–194.

STAICU, A.-M., CRAINICEANU, C. M., REICH, D. S. and RUPPERT, D. (2012). Modeling functional data with spatially heterogeneous shape characteristics. *Biometrics* **68** 331–343. MR2959599

STEIN, M. L. (1999). *Interpolation of Spatial Data*: *Some Theory for Kriging*. Springer, New York. MR1697409

STEIN, M. L. (2005). Space–time covariance functions. *J. Amer. Statist. Assoc.* **100** 310–321. MR2156840

SUN, Y., LI, B. and GENTON, M. G. (2012). Geostatistics for large datasets. In *Advances and Challenges in Space–Time Modelling of Natural Events* (E. Porcu, J. M. Montero and M. Schlather, eds.) **3** 55–77. Springer, Berlin.

THÉBAULT, E., FINLAY, C. C., BEGGAN, C. D., ALKEN, P., AUBERT, J., BARROIS, O., BERTRAND, F., BONDAR, T., BONESS, A., BROCCO, L., CANET, E., CHAMBODUT, A., CHULLIAT, A., COÏSSON, P., CIVET, F., DU, A., FOURNIER, A., FRATTER, I., GILLET, N., HAMILTON, B., HAMOUDI, M., HULOT, G., JAGER, T., KORTE, M., KUANG, W., LALANNE, X., LANGLAIS, B., LÉGER, J.-M., LESUR, V., LOWES, F. J., MACMILLAN, S., MANDEA, M., MANOJ, C., MAUS, S., OLSEN, N., PETROV, V., RIDLEY, V., ROTHER, M., SABAKA, T. J., SATURNINO, D., SCHACHTSCHNEIDER, R., SIROL, O., TANGBORN, A., THOMSON, A., TØFFNER-CLAUSEN, L., VIGNERON, P., WARDINSKI, I. and ZVEREVA, T. (2015). International geomagnetic reference field: The 12th generation. *Earth, Planets and Space* **67** 1–19.

ULICH, T., CLILVERD, M. A. and RISHBETH, H. (2003). Determining long-term change in the ionosphere. *Eos, Transactions American Geophysical Union* **84** 581–585.

YANG, J., ZHU, H., CHOI, T. and COX, D. D. (2016). Smoothing and mean-covariance estimation of functional data with a Bayesian hierarchical model. *Bayesian Anal.* **11** 649–670. MR3498041

YAO, F., MÜLLER, H.-G. and WANG, J.-L. (2005). Functional data analysis for sparse longitudinal data. *J. Amer. Statist. Assoc.* **100** 577–590. MR2160561

A. GROMENKO
IBM RESEARCH
9 CHANGI BUSINESS PARK CENTRAL 1
THE IBM PLACE
SINGAPORE 486048
SINGAPORE
E-MAIL: agromenko@gmail.com

P. KOKOSZKA
DEPARTMENT OF STATISTICS
COLORADO STATE UNIVERSITY
FORT COLLINS, COLORADO 80523
USA
E-MAIL: Piotr.Kokoszka@colostate.edu

J. SOJKA
DEPARTMENT OF PHYSICS
AND CENTER FOR ATMOSPHERIC AND SPACE SCIENCE
UTAH STATE UNIVERSITY
LOGAN, UTAH 84322-4405
USA
E-MAIL: sojka@cc.usu.edu